Engineering the Electronic Band Structure for Multiband Solar Cells

N. López, L. A. Reichertz, K. M. Yu, K. Campman, and W. Walukiewicz

Phys. Rev. Lett. **106**, 028701 — Published 10 January 2011

DOI: 10.1103/PhysRevLett.106.028701

Engineering of the Electronic Band Structure for Multiband Solar Cells

N. López[1], L. A. Reichertz[1,2], K. M. Yu[1], K. Campman[3], and W. Walukiewicz[1,2]

[1]*Materials Sciences Division, Lawrence Berkeley National Laboratory, 1 Cyclotron Road, Berkeley, CA 94720, USA*

[2] *RoseStreet Labs Energy, 3701 E. University Drive, Phoenix, AZ 85034 USA*

[3]*Sumika Electronic Materials, Inc., 3832 E. Watkins Street, Phoenix, AZ 85034 USA*

Using the unique features of the electronic band structure of GaN_xAs_{1-x} alloys, we have designed, fabricated and tested a multiband photovoltaic device. The device demonstrates an optical activity of three energy bands that absorb, and convert into electrical current, the crucial part of the solar spectrum. The performance of the device and measurements of electroluminescence, quantum efficiency and photomodulated reflectivity are analyzed in terms of the Band Anticrossing model of the electronic structure of highly mismatched alloys. The results demonstrate the feasibility of using highly mismatched alloys to engineer the semiconductor energy band structure for specific device applications.

PACS 88.40.fh, 84.60.Jt, 72.40.+w, 78.60.Fi

In order to increase the efficiency and overcome the Schockley-Queisser limit [1], a number of new concepts of solar cells have been proposed. In the most successful approach several solar cells using semiconductors with different energy gaps are connected in series in a multijunction or tandem device structure [2]. Most recently efficiencies exceeding 40% were realized with three junction solar cells under concentration [3, 4]. A great disadvantage of this design is the complexity of the structure and the device fabrication process. It has been proposed [5-10] that a better utilization of the full solar spectrum could be also achieved with one or more narrow, intermediate bands (IB) properly located in the bandgap of a wide gap semiconductor. The IBs act as stepping stones allowing low energy photons to transfer electrons from the valence band (VB) to the conduction band (CB). The key advantage of such multiband or intermediate band solar cell (IBSC) would be its simplicity as it requires a single p-n junction only. There were several proposals of multiband materials including short period superlattice structures [11-13] or transition metal doped semiconductors [14]. However, despite a considerable effort of many research groups there has been no evidence of a working multiband photovoltaic device.

In this letter we describe how tailoring of the electronic band structure of highly mismatched alloys can be used to design semiconductor materials for specific device applications. Using GaNAs alloys we were able successfully realize an intermediate band photovoltaic device.

Highly mismatch alloys (HMAs) are a new class of materials formed through alloying of distinctly different semiconductors [15]. Dilute nitrides (oxides) in which column V (VI) atoms in a standard group III-V (II-VI) compounds are partially replaced

with nitrogen (oxygen) are the most prominent and extensively studied HMAs [16-21]. The band structure of HMAs is well described by the Band Anticrossing (BAC) model [15, 16] which has shown that some of the dilute nitrides or oxides exhibit unusual energy band structure with a narrow band of states located in the band gap of the host material [21-23] indicating that such HMAs could be used for multiband solar cells. Here we report on a practical realization of the IBSC concept using dilute nitride HMAs.

The key requirement for an IBSC is that the IB is isolated from the charge collecting contacts assuring that the operational voltage is determined by the largest band gap. In order to satisfy this condition we have designed device structures with and without layers blocking charge transport in the IB. The device structures are shown in Figs. 1(a) and (b). The figures also show the energy band diagram calculated using a Poisson equation solver [24]. The energy band structure of the GaN_xAs_{1-x} layers was calculated using the BAC model [15, 16].

The structure with Blocked Intermediate Band (BIB) shown in Fig. 1(a) has the blocking layers on both the surface and the substrate side whereas the structure with Unblocked Intermediate Band (UIB) shown in Fig. 1(b) has the IB connected to the substrate side of the device. The UIB device plays the role of a reference sample.

The n-type doping of the GaN_xAs_{1-x} layer results in a partial occupation of IB assuring optical transitions to and from the IB [25]. The optical transitions contributing to the photocurrent and the carrier recombination paths are shown in Figs. 1(a) and (b). An electron hole pair can be generated directly by absorption of one photon ($h\nu_3$) with the energy larger than the band gap, E_C-E_V, or in a two step process involving two lower

energy photons promoting optical transitions from the VB to the IB ($h\nu_2$) and from the IB to the CB ($h\nu_1$).

The device structures used in the current study were fabricated utilizing metalorganic chemical vapor deposition (MOCVD). The photovoltaic devices were fabricated with standard ohmic contacts to heavily n-type doped substrates and p-type doped surface layers. The composition x=0.024 has been determined from PR measurements using the BAC model. Special precautions were taken to provide for efficient sample cooling in the electroluminescence experiments.

The measured external quantum efficiencies (EQE) for BIB and UIB devices are shown in Fig. 2(a). In the UIB device the photocurrent shows an abrupt onset at 1.1 eV followed by a maximum for photon energy close to the transition between the VB and the IB and a rapid decay at higher photon energies. In a stark contrast, in the BIB device the photocurrent clearly exhibits two thresholds; the first at about 1.1 eV and the second at 2 eV, corresponding to the transitions from VB to IB and VB to CB, respectively. As seen in Fig. 2(b) we find an excellent agreement of the EQE thresholds with VB to IB and VB to E_+ (CB) transitions measured by photomodulated reflection (PR). Note that the transition from IB to E_+ cannot be resolved.

The EQE results are fully consistent with the expected behavior of the transport of photoexcited charge carriers in the structures shown in Figs. 1(a) and (b). In the UIB device, electrons excited to either the IB or the CB are collected at the back substrate side whereas the VB holes are driven to the surface contact. The IB plays the role of the conduction band and the device acts as a single gap photovoltaic cell whose characteristics are determined by the band gap of about 1.1 eV between the IB and the

VB. On the other hand, in the BIB device shown in Fig. 1(a) the backside blocking layer prevents transfer of electrons from the IB to the back contact. Under broad band solar illumination the electrons photoexcited from the VB to the IB absorb another low energy photon and are transferred to the CB to be collected at the back contact. Note that the low energy EQE threshold for this process is given by $h\nu_2$, i.e. the larger of the two photon energies. This is because in order to generate an electron in CB and a hole in the VB the two types of transitions from VB to the IB ($h\nu_2$) and from the IB to CB ($h\nu_1$) have to be possible. The higher energy threshold at 2 eV is observed when photon energy is large enough to excite electron from VB directly to CB.

Further support for the multiband operation of our device is provided by measurements of the current voltage (I/V) characteristics. The I/V curves for the two types of structures obtained under solar spectrum illumination with the intensity of about 20xAM1.5 are shown in Fig 3. The UIB structure shows an open circuit voltage (V_{oc}) of about 0.42 V whereas the BIB structure has a significantly higher V_{oc} of 0.92 V. In general, the V_{oc} of a PV device depends on the band gap, E_g, and is given by $V_{oc}=(E_g-\Delta)/e$. The offset Δ depends on the junction and material quality as well as the sunlight concentration factor and has been shown to be larger than 0.4 eV under 1 sun illumination [26]. The small V_{oc} and large value of Δ=0.68 eV in the UIB structure is consistent with a relatively poor quality junction in a semiconductor with E_g=1.1 eV. However the large, more than two fold increase of V_{oc} in the BIB structure can be only associated with a gap much larger 1.1 eV, confirming our expectations that the largest band gap of 2 eV between CB and VB is responsible for the charge separation in this

structure. The large value of the offset Δ found in both cases is most likely related to a short minority carrier lifetime as has been previously found in GaInNAs alloys [27].

All the above results indicate that the BIB structure operates as a multiband PV device. Such a structure is expected to operate also as a light emitter under applied external voltage. Low temperature (15 K) measurements of the electroluminescence (EL) in the BIB and UIB devices are shown in Fig. 4. The BIB structure shows four EL peaks whereas the UIB device shows only one strong EL peak. In order to understand the difference in the EL spectra one needs to analyze the electric field distribution in the BIB and UIB structures. In a semiconductor light emitting device EL originates from regions of the samples where an external bias can produce a large enough electric field to inject electrons to the CB and holes to the VB. It is evident from Fig. 1(a) that in the BIB structure the voltage drop of an externally applied forward bias occurs in two depletion regions: (i) the p/n junction depletion region in GaNAs close to the surface and (ii) the region next to the backside $Al_{0.45}Ga_{0.55}As$ blocking layer. On the other hand, in the UIB device there is only a potential drop in the GaNAs p/n junction depletion region because there is no blocking barrier between the CB of the substrate and the IB of GaNAs. Consequently, when a forward voltage is applied to the BIB structure, holes are injected from the surface contact into the n-GaNAs layer whereas electrons are injected from the n-GaAs substrate into the GaNAs CB. As a result, two emission peaks are observed, the low energy peak at about 0.9 eV from radiative recombination between the CB and the partially occupied IB, and the peak at 1.15 eV from transitions between the partially occupied IB and the VB. The energy of the later peak is in good agreement with the energy gap between IB and VB calculated by the BAC model and determined from EQE

and PR measurements shown in Fig. 2(a) and (b) respectively. The low energy peak at 0.9 is also in good agreement with the energy separation between CB and IB calculated for the GaN_xAs_{1-x} layer. It is worth noting that because of the partial occupation of the IB, those two peaks can be also observed in the reverse bias.

As seen in Fig. 4 the UIB structure shows only a single EL peak with the energy corresponding to the transitions from IB to VB. The absence of the low energy peak can again be attributed to the fact that there is no potential drop at the interface with the GaAs substrate and therefore electrons cannot be injected into the CB.

Regarding the origin of the two high energy EL peaks in the BIB structure we note that they have to originate from the depletion region at the backside interface where holes from GaNAs are injected into the n-GaAs substrate. The EL peak at about 1.47 eV can be attributed to GaAs band edge emission and the peak at 1.35 eV to a defect related emission in this heavily doped substrate. This explanation is fully consistent with the absence of these high energy peaks in the UIB device where there is no potential drop at the backside interface and holes cannot be injected into the GaAs substrate.

The key result of the EL experiments is the first demonstration of the optical transitions between CB and IB providing a missing link to a fully operational multiband (or IB) PV device. It emphasizes the importance of the blocking of the charge transport in the intermediate band.

Material growth and device design and fabrication were supported by RoseStreet Labs Energy. The EL work performed at LBNL was supported by the Director, Office of Science, Office of Basic Energy Sciences, Materials Sciences and Engineering Division,

of the U.S. Department of Energy under Contract No. DE-AC02-05CH11231. N. López also acknowledges the financial support of the Ministerio de Ciencia e Innovación of the Spanish Government.

References

[1] W. Shockley and H. J. Queisser, Journal. Appl. Phys. **32**, 510 (1961).

[2] J. M. Olson, D. J. Friedman and Sarah Kurtz, in *Handbook of Photovoltaic Science and Engineering*. Edited by A. Luque and S. Hegedus (Wiley & Sons, 2003) Chapter 9, p. 359.

[3] W.Guter et al., Applied Physics Letter **94**, 223504 (2009).

[4] J.F. Geisz et al., Applied Physics Letter **93**, 123505 (2008).

[5] M. Wolf, Proc. IRE **48**, 1246 (1960).

[6] A. Luque and A. Martí, Physical Review Letters **78**, 5014–5017 (1997).

[7] A. M. Green, Progress in Photovoltaics: Research and Applications **9**, 137 (2001).

[8] A. Vos and H. Pauwels, Applied Physics A: Materials Science & Processing **25**, 119-125 (1981).

[9] A. Luque and A. Martí, Progress in Photovoltaics: Res. Appl. **9**, 73–86 (2001).

[10] A. Martí, L. Cuadra and A. Luque, IEEE Transactions on Electron Devices **49**, 1632–1639 (2002).

[11] A. M. Green, Materials Science and Engineering B **74**, 118–124 (2000).

[12] R. J. Chaffin, et al., Conf. Record 17th IEEE Photovoltaic Specialists Conference, Kissimmee, 743–746 (1984).

[13] A. Luque et al., Applied Physics Letters **87**, 083505 (2005).

[14] K. Sánchez, et al., Physical Review B **79**, 165203 (2009).

[15] W. Walukiewicz et al., Physical Review Letters. **85**, 1552 (2000).

[16] W. Shan et al., Physical Review Letters **82**, 1221-1224 (1999).

[17] M. Weyers, M. Sato and H. Ando, Japan Journal of Applied Physics. **31**, L853 (1992).

[18] J. N. Baillargeon, K. Y. Cheng, G. E. Hofler, P. J. Pearah, K. C. Hsieh, Applied Physics Letters **60**, 2540 (1992).

[19] W. G. Bi, C. W. Tu, Applied Physics **80**, 1934 (1996).

[20] W. Shan et al., Physical Review B **62**, 4211 (2000).

[21] K. M. Yu et al., Physical Review Letters **91**, 246403-4 (2003).

[22] K. M. Yu et al., Applied Physics Letters **88**, 092110-3 (2006).

[23] J. F.Geisz, D. J.Friedman and Semicond, Science. Technologic. **17**, 769 (2002).

[24] M. Burgelman, P. Nollet and S. Degrave, Thin Solid Films **361-362**, 527-532 (2000).

[25] A. Martí, L. Cuadra and A. Luque, IEEE Transactions on Electron Devices **48**, 2394–2399 (2001).

[26] R. R. King et al., Applied Physics Letters **90**, 183516 (2007).

[27] D. J. Friedman, J. F. Geisz, S. R. Kurtz, J. M. Olson, J. of Crys. Growth **195**, 409 (1998).

FIGURE CAPTIONS

Fig.1. (Color online) (a) The structure and band diagram of a BIB device with the intermediate band (IB) disconnected from the contacts. Transitions generating electron-hole pairs utilizing IB are denoted as $h\nu_1$, $h\nu_2$. The transitions from VB to CB are represented by $h\nu_3$. (b) The structure and the band diagram of an UIB device with the IB connected to the backside contact. The electron affinity values for AlGaAs and InGaP are 3.63 and 4.1 eV respectively.

Fig. 2. (Color online) (a) The spectral dependence of the external quantum efficiency. The solid line represents the EQE response for the BIB device and the dashed line corresponds to the UIB device. (b) Photomodulated reflectivity measured on the BIB device.

Fig. 3. (Color online) Current density vs. voltage curve measured on BIB (solid line) and UIB (dashed line) structure.

Fig. 4. (Color online) Electroluminescence measurements at low temperature (15K) for BIB (solid line) and UIB (dashed line).

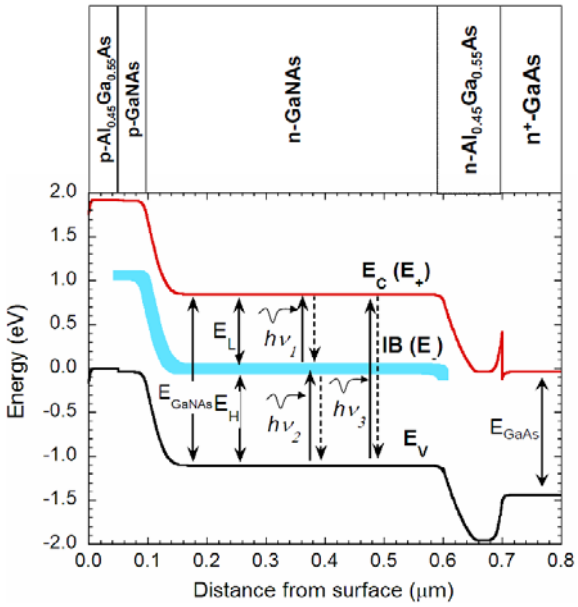

(a)

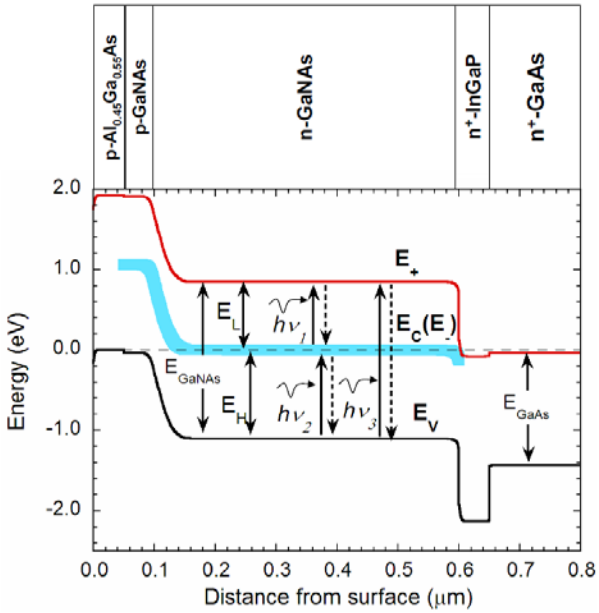

(b)

Fig.1. (Color online) (a) The structure and band diagram of a BIB device with the intermediate band (IB) disconnected from the contacts. Transitions generating electron-hole pairs utilizing IB are denoted as $h\nu_1$, $h\nu_2$. The transitions from VB to CB are represented by $h\nu_3$. (b) The structure and the band diagram of an UIB device with the IB connected to the backside contact. The electron affinity values for AlGaAs and InGaP are 3.63 and 4.1 eV respectively.

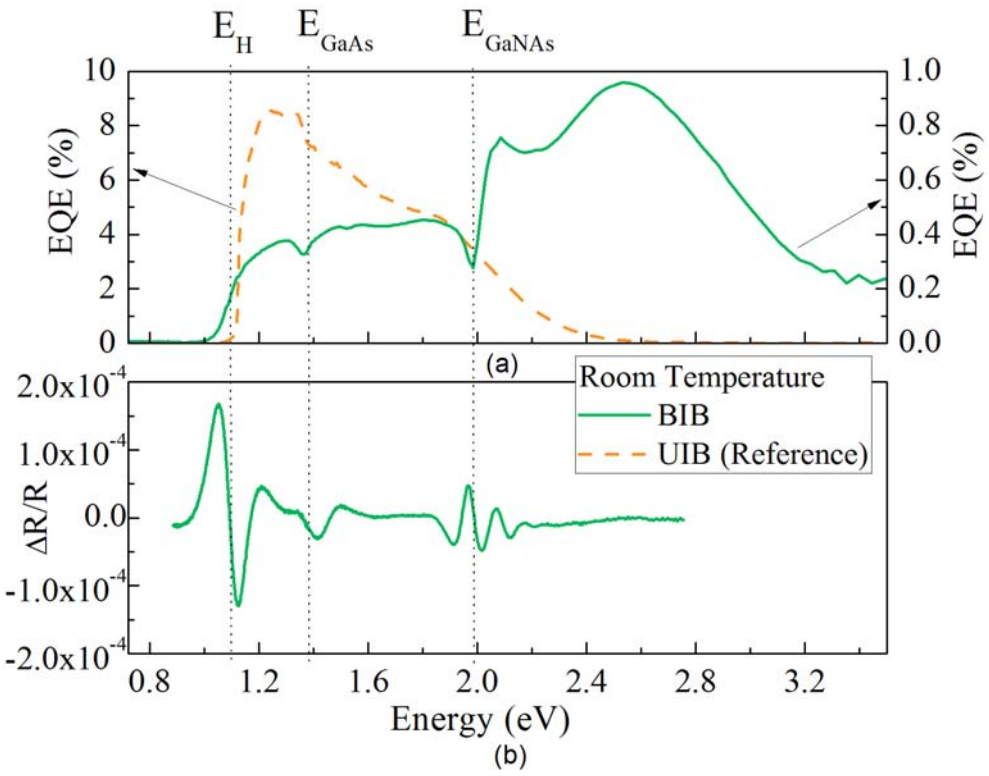

Fig. 2. (Color online) (a) Spectral dependence of the external quantum efficiency. The solid line represents the EQE response for the BIB device and the dashed line corresponds to the UIB device. (b) Photomodulated reflectivity measured on the BIB device.

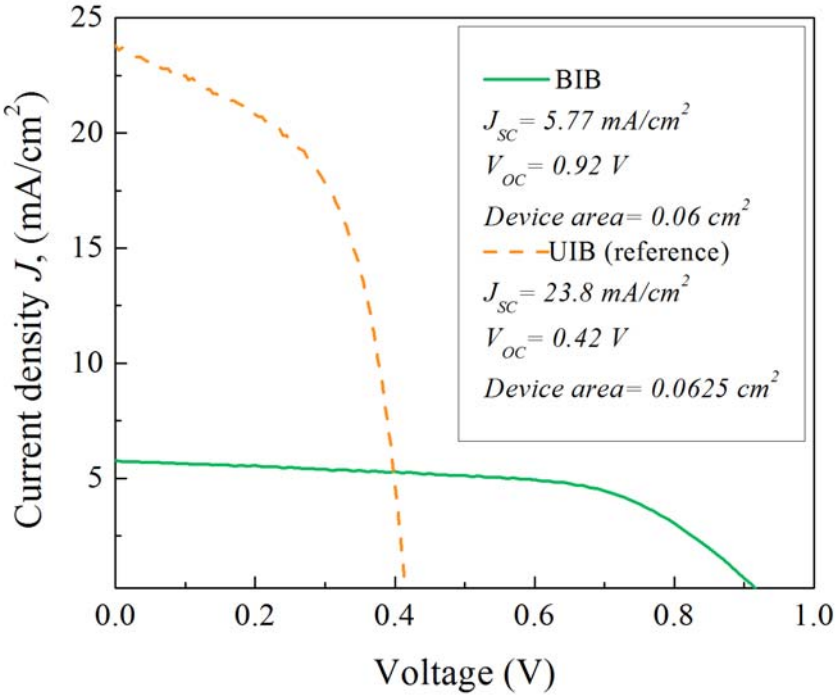

Fig. 3. (Color online) Current density vs. voltage curve measured on BIB (solid line) and UIB (dashed line) structure.

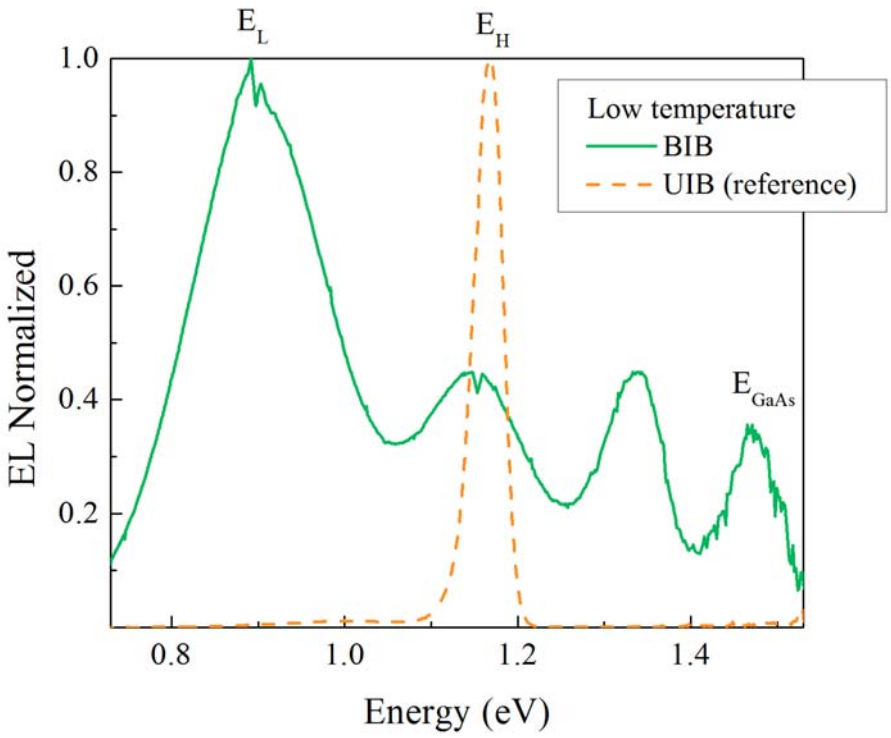

Fig. 4. (Color online) Electroluminescence measurements at low temperature (15K) for BIB (solid line) and UIB (dashed line).